

The physical connection between central stellar surface density and stellar spin in SAMI and MaNGA nearby galaxies

L. Cortese,^{1,2*} A. Fraser-McKelvie,^{1,2} J. Woo,³ B. Catinella,^{1,2} K. Harborne,^{1,2} J. van de Sande,^{2,4}
J. Bland-Hawthorn,^{2,4} S. Brough,^{2,5} J. J. Bryant^{2,4,6} S. Croom,^{2,4} S. Sweet^{2,7}

¹International Centre for Radio Astronomy Research, The University of Western Australia, 35 Stirling Hw, 6009 Crawley, Australia

²ARC Centre of Excellence for All Sky Astrophysics in 3 Dimensions (ASTRO 3D), Australia

³Department of Physics, Simon Fraser University, 8888 University Drive, Burnaby, BC V5A 1S6, Canada

⁴Sydney Institute for Astronomy (SIfA), School of Physics, The University of Sydney, NSW 2006, Australia

⁵School of Physics, University of New South Wales, NSW 2052, Australia

⁶Australian Astronomical Optics, AAO-USydney, School of Physics, University of Sydney, NSW 2006, Australia

⁷School of Mathematics and Physics, University of Queensland, Brisbane, QLD 4072, Australia

Accepted XXX. Received YYY; in original form ZZZ

ABSTRACT

The stellar surface density within the inner 1 kpc (Σ_1) has become a popular tool for understanding the growth of galaxies and its connection with the quenching of star formation. The emerging picture suggests that building a central dense core is a necessary condition for quenching. However, it is not clear whether changes in Σ_1 trace changes in stellar kinematics and the growth of dispersion-dominated bulges. In this paper, we combine imaging from the Sloan Digital Sky Survey with stellar kinematics from the Sydney-AAO Multi-object Integral-field unit (SAMI) and Mapping Nearby Galaxies at Apache Point Observatory (MaNGA) surveys to quantify the correlation between Σ_1 and the proxy for stellar spin parameter within one effective radius (λ_{re}) for 1599 nearby galaxies. We show that, on the star-forming main sequence and at fixed stellar mass, changes in Σ_1 are mirrored by changes in λ_{re} . While forming stars, main sequence galaxies remain rotationally-dominated systems, with their Σ_1 increasing but their stellar spin staying either constant or slightly increasing. The picture changes below the main sequence, where Σ_1 and λ_{re} are no longer correlated. Passive systems show a narrower range of Σ_1 , but a wider range of λ_{re} compared to star-forming galaxies. Our results indicate that, from a structural point of view, passive galaxies are a more heterogeneous population than star-forming systems, and may have followed a variety of evolutionary paths. This also suggests that, if dispersion-dominated bulges still grow significantly at $z \sim 0$, this generally takes place during, or after, the quenching phase.

Key words: galaxies: evolution – galaxies: disc – galaxies: bulges – galaxies: kinematics and dynamics – galaxies: photometry

1 INTRODUCTION

One hundred years since its conception, understanding the physical origin of the Hubble morphological sequence of galaxies (Hubble 1926) remains one of the major challenges for extragalactic astronomy. While relatively simple in its original definition, the Hubble ‘tuning fork’ simultaneously traces changes in star formation activity (e.g., prominence of spiral arms) and stellar structure (e.g., presence of stellar bulges and/or bars), making its physical interpretation not always straightforward. Thus, it is not surprising that, throughout the decades, various re-incarnations of the Hubble tuning fork have been proposed (e.g., de Vaucouleurs 1959; Cappellari et al. 2011b; Kormendy & Bender 2012), with an effort to provide more physical basis to the initial visual criteria used to separate different morphological types (see also Romanowsky & Fall 2012; Cortese et al. 2016; Hardwick et al. 2022).

Even when the focus is on stellar structure alone, the complexity of the galaxy ecosystem can make it difficult to link visual mor-

phology to the actual orbital distribution of stars (e.g., Zhu et al. 2018). This is showcased, for example, by the degeneracy in the use of the term ‘bulge’ in the context of galaxy evolution. From a physical point of view, it is generally assumed that this should be a structural component different from a disk, where most (if not all) the dynamical support comes from non circular orbits (now-a-days referred to as ‘classical bulge’). In reality, most works use this term to simply identify deviations in central light surface brightness/mass surface density from what is expected from an exponential disk (e.g. Kent 1985; Peng et al. 2002; Simard et al. 2011; Lange et al. 2016). This culminates with the use of the term ‘pseudo-bulge’ to indicate features with a disc-like 2D structure at the centre of galaxies (Kormendy & Kennicutt 2004; Erwin et al. 2015). In addition, the exact quantification of the properties of the ‘bulge’ heavily depends on the technique used to separate this component from a disk (Kormendy & Bender 2012; Meert et al. 2015; Cook et al. 2019; Tabor et al. 2019; Oh et al. 2020), potentially hampering our ability to unveil the evolutionary history of the inner parts of galaxies.

An alternative approach is to refrain from trying to separate the ‘bulge’ from the disc using 2D imaging observations and instead

* E-mail: luca.cortese@uwa.edu.au (LC)

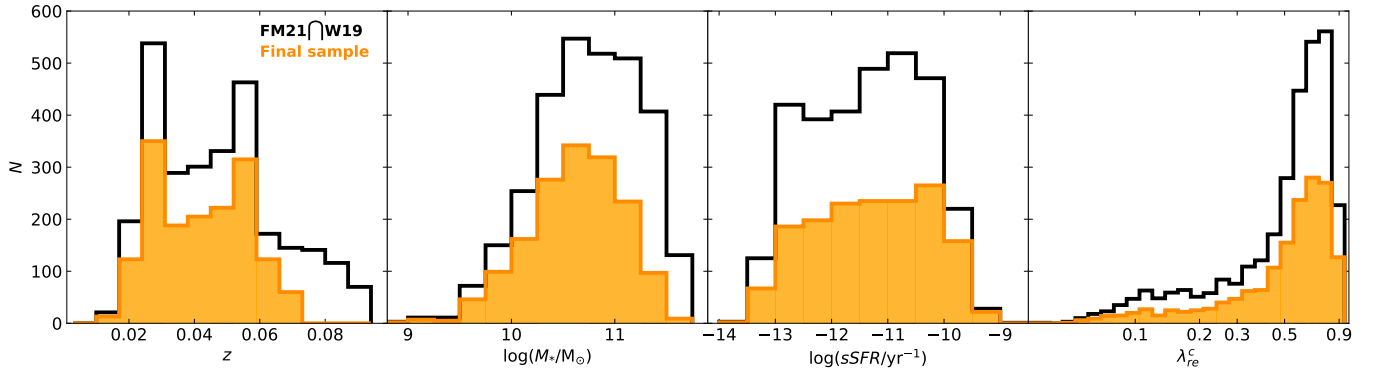


Figure 1. The distributions of (from left to right) redshift (z), stellar mass (M_*), specific star formation rate ($sSFR \equiv SFR/M_*$) and stellar spin parameter within one effective radius ($\lambda_{r_e}^c$) for our final sample (filled orange histograms). The empty black histograms show the distribution of our parent sample extracted from the intersection of the SAMI+MaNGA sample of Fraser-McKelvie et al. (2021) and the Σ_1 SDSS catalogue of Woo & Ellison (2019).

quantify how much, and how fast, the central core of galaxies grows. Specifically, in recent years, parts of the community have focused on the central stellar surface density of galaxies, generally measured within the central 1 kpc (Σ_1 , Cheung et al. 2012). Being a non-parametric quantity, Σ_1 is independent of the actual nature of the central core of galaxies and, compared to the historically more popular stellar surface density within one effective radius, is less sensitive to changes in disk properties at larger radii, and supposed to trace the growth of the central core of galaxies (Fang et al. 2013; Barro et al. 2017; Walters et al. 2021).

The popularity of Σ_1 has further increased due to the fact that it appears to be one of the best structural parameters able to discriminate between active and passive galaxies. As initially shown by Cheung et al. (2012) and Barro et al. (2017), and then confirmed by several others (e.g., Tacchella et al. 2015; Whitaker et al. 2017; Mosleh et al. 2017; Woo et al. 2015, 2017; Woo & Ellison 2019; Wang et al. 2018; Chen et al. 2020; Suess et al. 2021), there appears to be a clear threshold in the value of Σ_1 above which galaxies are almost always quiescent. This has provided indirect support to a scenario in which the growth of the central stellar core in galaxies may be physically linked to the process driving quenching (e.g., the growth of the central supermassive black hole and the onset of feedback from active galactic nuclei, AGN), a process sometimes referred to as ‘compaction’ (Zolotov et al. 2015; Tacchella et al. 2015). While, from a theoretical point of view, compaction is expected to be more important at high redshift, recent works have suggested that it may also be an effective mechanism in the local galaxy population (e.g., Wang et al. 2018).

While the quantification of the correlation between Σ_1 , stellar mass, star formation rate (SFR) and other galaxy properties, as well as their dependence on redshift, has now been well established, the interpretation of the correlations in the framework of galaxy transformation, and specifically compaction, remains challenging. This is due, once again, to the fact that a higher value of Σ_1 at fixed other galaxy properties may be blindly assumed as evidence for the build-up of a dispersion-supported structure. This would require invoking specific physical processes able to alter the orbital structure of stars in the disc (e.g., mergers or violent disc instability, Noguchi 1999). However, it has never been demonstrated whether or not Σ_1 is a good proxy for the presence of classical bulges in galaxies. Could it be that Σ_1 simply traces the stellar mass growth of discs? Is the link between

Σ_1 and star formation quenching truly a by-product of the build-up of dispersion-supported structures in the core of galaxies?

There are very good reasons to expect that Σ_1 may not always trace the presence of classical bulges. Indeed, we already know that, at high stellar mass and stellar surface density, galaxies show a wide range of kinematic properties, as highlighted by the ATLAS 3D survey (Cappellari et al. 2011a), and confirmed by more recent integral field spectroscopic (IFS) surveys (Cortese et al. 2016; van de Sande et al. 2018; Falc3n-Barroso et al. 2019; Wang et al. 2020; Guo et al. 2020). With the advent of large IFS surveys it is paramount that we start to include kinematic information in our characterisation of galaxy structure. In particular, stellar kinematics are critical for discriminating between classical bulges and disc-like structures at the centre of galaxies.

A wide range of stellar kinematic properties at fixed Σ_1 would impact on the use of the mass-SFR- Σ_1 plane to constrain the various paths to quiescence followed by galaxies. Indeed, the narrow range of Σ_1 observed in passive systems has sometimes been used to suggest a very narrow range of evolutionary paths (and thus physical processes) leading to quiescence (Barro et al. 2017; Woo & Ellison 2019; Suess et al. 2021). Of course, if this limited range was just the result of the inability of Σ_1 to discriminate between discs and bulges in the inner 1 kpc of galaxies, this would have major implications on our view of galaxy evolution.

To address this issue, in this paper we present a detailed analysis of the correlation between central stellar surface density Σ_1 and stellar spin parameter for a sample of galaxies extracted from the overlap of the Sloan Digital Sky Survey (SDSS, York et al. 2000), and the Mapping Nearby Galaxies at Apache Point Observatory (MaNGA, Bundy et al. 2015) and SAMI (Bryant et al. 2015; Croom et al. 2021a) IFS surveys. Our study extends on previous works that looked at the correlation between Σ_1 and central stellar velocity dispersion (e.g., Fang et al. 2013; Chen et al. 2020) by exploiting the resolved stellar kinematics maps provided by SAMI and MaNGA.

This paper is organised as follows. In Section 2, we describe our sample selection and estimates of Σ_1 and stellar spin, as well the ancillary data used in this work. In Section 3, we look at the correlation between Σ_1 and stellar spin for star-forming and passive galaxies, separately. This section includes the main results of this work. Lastly, we discuss the implications of our results in Section 4 and summarise in Section 5. Throughout this paper, we use a flat Λ

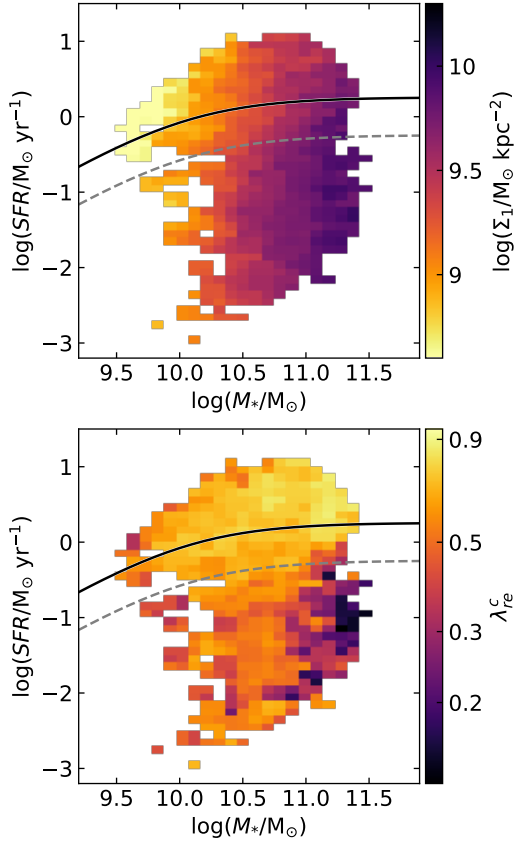


Figure 2. The SFR- M_* plane for our sample color-coded by the median value of Σ_1 (top panel) and λ_{re}^c (bottom panel). Medians are calculated in steps of 0.1 dex including all galaxies within 0.2 dex in both stellar mass and SFR. The solid line shows the best-fit to the star-forming main sequence of Fraser-McKelvie et al. (2021), with the dashed line indicating the threshold used here to separate star-forming and passive galaxies. Only bins with five or more galaxies are shown.

cold dark matter concordance cosmology: $H_0 = 70 \text{ km s}^{-1} \text{ Mpc}^{-1}$, $\Omega_M = 0.3$ and $\Omega_\Lambda = 0.7$.

2 SAMPLE SELECTION

Our parent sample is taken from Fraser-McKelvie et al. (2021), who combined stellar kinematic measurements from both the SAMI and MaNGA surveys for a sample of 3289 nearby galaxies over a stellar mass range $9.5 < \log(M_*/M_\odot) < 12$ and up to at least one effective radius. Briefly, galaxies are extracted from the overlap of the two surveys with the GALEX-SDSS-WISE Legacy Catalog (GSWLC, version 2; Salim et al. 2016) to guarantee homogeneous estimates of global stellar masses and current SFRs across the redshift range and stellar mass regimes covered by both surveys. We start from the stellar line-of-sight velocities and velocity dispersion maps produced by the SAMI (van de Sande et al. 2017) and MaNGA (Westfall et al. 2019) teams, which have been extracted from data cubes adaptively binned to a signal-to-noise of 10 using the Voronoi binning code of Cappellari & Copin (2003). The stellar flux-weighted spin parameter proxy within one effective radius (λ_{re}) was estimated from the line-of-sight and velocity dispersion maps following the definition presented in Emsellem et al. (2007), with Petrosian r -band effective radii obtained from the NASA-Sloan Atlas (Blanton et al. 2011). In

order to correct for the effect of both beam smearing and inclination we proceeded as follows. First, λ_{re} estimates were corrected for beam smearing following the empirical recipes presented in Harborne et al. (2020), which are based on seeing and Sersic index. Beam-smearing corrected spin values were then corrected for inclination using the r -band ellipticity value as a proxy for inclination following del Moral-Castro et al. (2020). We point the reader to Fraser-McKelvie et al. (2021) and van de Sande et al. (2021) for an extensive discussion of these corrections. In the following, we use the corrected value λ_{re}^c as a proxy for the stellar spin parameter, but we note that the main conclusions of this paper do not qualitatively change if observed (i.e., not corrected for either beam smearing or inclination) values are used, as discussed in Appendix A of this paper.

We cross-correlated the SAMI+MaNGA sample with the measurements of central stellar surface density (Σ_1) presented in Woo & Ellison (2019). These have been obtained by converting the SDSS surface brightness profiles in g and i band into stellar surface density profiles using the stellar mass-to-light color relation presented in Fang et al. (2013). Σ_1 is then obtained by interpolating the stellar mass profiles and measuring the total stellar mass within 1 kpc. While $\sim 95\%$ of the galaxies in our IFS sample are included in the parent sample of Woo & Ellison (2019) (3102 out of 3289), for a good fraction of them 1 kpc is smaller than the point-spread function (PSF) of SDSS observations. Thus, to remove objects for which the estimate of Σ_1 could be unreliable and/or biased, we focus on galaxies with $z < 0.07$, for which the PSF of SDSS images corresponds to less than 1 kpc, and exclude highly inclined systems (i.e., minor-to-major axis ratio $b/a < 0.5$). Residual seeing effects do not affect our conclusions, as discussed in Appendix B. These cuts reduce the overlap with the IFS sample to 1599. While the sample decreases by a factor of ~ 2 in size, we note that our final sample still spans the same parameter space in stellar mass, specific SFR and stellar spin parameter as the whole sample, as clearly shown in Fig. 1. As expected, the redshift cut primarily affects our ability to sample the very high stellar mass regime ($M_* \gtrsim 10^{11.5} M_\odot$).

Throughout this paper, we investigate galaxies on and below the star-forming main sequence (SFMS) separately. We use the best fit to the SFMS presented by Fraser-McKelvie et al. (2021). This was calculated using all galaxies in SAMI and MaNGA with SFRs included in the GSWLC catalog:

$$\log(SFR_{MS}) = 0.256 - \log\left(1 + \frac{10^{10.064}}{M_*}\right) \quad (1)$$

Our active population includes all galaxies whose SFR is higher than $SFR_{MS} - 0.5$ dex (see Fig. 2, 720 galaxies), whereas the passive population includes all galaxies with SFR below this threshold (879 galaxies).

3 THE CONNECTION BETWEEN STELLAR CENTRAL SURFACE DENSITY AND SPIN

We start by showing in Fig. 2 the SFR- M_* plane covered by our sample, color-coded by the median value of Σ_1 (top panel) and λ_{re}^c (bottom panel)¹. We divided this plane into a grid with pixels 0.1 dex wide. For each pixel, we show the median value for all galaxies with

¹ In this paper, we treat λ_{re}^c as a log-normally distributed quantity and plot it in log scale. While this may seem at odds with what is generally done in the literature, where stellar spin is treated as a linear quantity, from a theoretical point of view the stellar spin is expected to follow a log-normal distribution (e.g., Mo et al. 1998; Bullock et al. 2001).

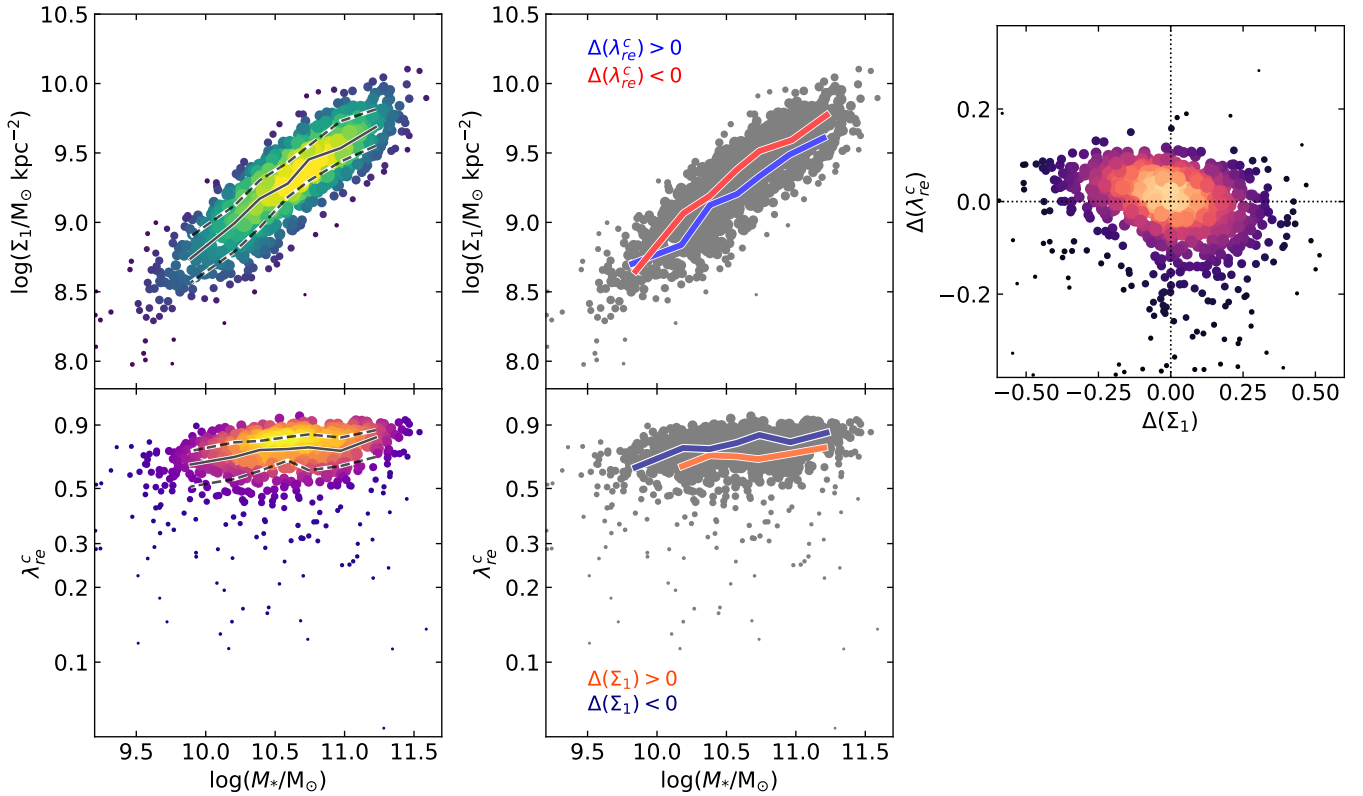


Figure 3. The correlation between Σ_1 and λ_{re}^c on the star-forming main sequence. *Left column.* The Σ_1 - M_* (top) and λ_{re}^c - M_* (bottom) for galaxies on the star-forming main sequence. Point size and color-coding reflect the probability density distributions of galaxies across each parameter space, with yellow/lighter colors indicating higher density. The black line shows the median relation for the whole sample, with dashed lines showing the 25% and 75% percentiles (see also Table C1). *Middle column.* Same as left column, with coloured lines now showing the running medians for galaxies with λ_{re}^c (top) or Σ_1 (bottom) higher/lower than the observed median value at fixed stellar mass. *Right.* Variation in λ_{re}^c as a function of variations in Σ_1 at fixed stellar mass. It is clear that, once we control for mass, an increase in central stellar surface density traces a decrease in stellar spin, and vice-versa.

stellar mass and SFR within 0.2 dex from the centre of each pixel. This means that we are oversampling the distribution of galaxies in this plane.

The comparison between the two panels of Fig. 2 already indicates that, while at fixed stellar mass passive galaxies have generally higher Σ_1 and lower λ_{re}^c than active systems, once we focus on either star-forming or quiescent populations alone changes in Σ_1 may not always be followed by changes λ_{re}^c , and vice-versa. To better quantify the differences between the two structural indicators, in the following we examine star-forming and quiescent galaxies, separately.

3.1 The star-forming main sequence

In Fig. 3, we show the Σ_1 - M_* (top left) and λ_{re}^c - M_* (bottom left) relations for all star-forming galaxies in our sample. Color-coding and symbol size scale with the probability density distributions of galaxies across both parameter spaces. The black solid line shows the running medians for both relationships, with dashed lines indicating the 25% and 75% interquartile ranges (see also Table C1).

As already shown by several authors in the last decade (e.g., Cheung et al. 2012; Fang et al. 2013; Suess et al. 2021), on the SFMS, Σ_1 monotonically increases with stellar mass. The slope of the correlation is clearly shallower than 1 implying that, if galaxies grow in mass moving *along* this relation (or following even shallower tracks as suggested by cosmological simulations, see e.g., Tacchella et al.

2016; Chen et al. 2020; Walters et al. 2021), most of the mass growth would take place in the outer parts of the disk (i.e., at radii larger than 1 kpc). In other words, galaxies would not become more compact (or more centrally concentrated) while on the SFMS. This simple speculation becomes even more interesting when we look at the distribution of stellar spin parameter as a function of stellar mass. Star-forming galaxies show a narrow range of stellar spins, with λ_{re}^c slightly increasing with mass (i.e., $\lesssim 0.1$ dex across 1 dex in M_* ; see Table C1), as already shown by Wang et al. (2020) and Fraser-McKelvie et al. (2021). From a structural point of view, SFMS galaxies appear to form a *disc main sequence*.

If we combine the top and bottom left panels of Fig. 3, it appears that, on the SFMS, the fact that more massive galaxies have a higher value of Σ_1 *does not* necessarily imply that they have a more prominent dispersion-supported central component (i.e., a classical bulge). On the contrary, despite having higher central surface densities than lower mass systems, high mass galaxies are still rotationally-dominated systems from a kinematic perspective (e.g., $\lambda_{re}^c > 0.5$). Intriguingly, this would be in line with the idea that most of the growth of mass on the SFMS at $z \sim 0$ takes place beyond 1 kpc, as already hinted from the slope of the $\Sigma_1 - M_*$ relation.

Now that we have established how both Σ_1 and λ_{re}^c vary with stellar mass, it is important to investigate whether or not these two structural parameters are correlated *at fixed mass*. After all, both scaling relations have a significant scatter (i.e., average 25% to 75%

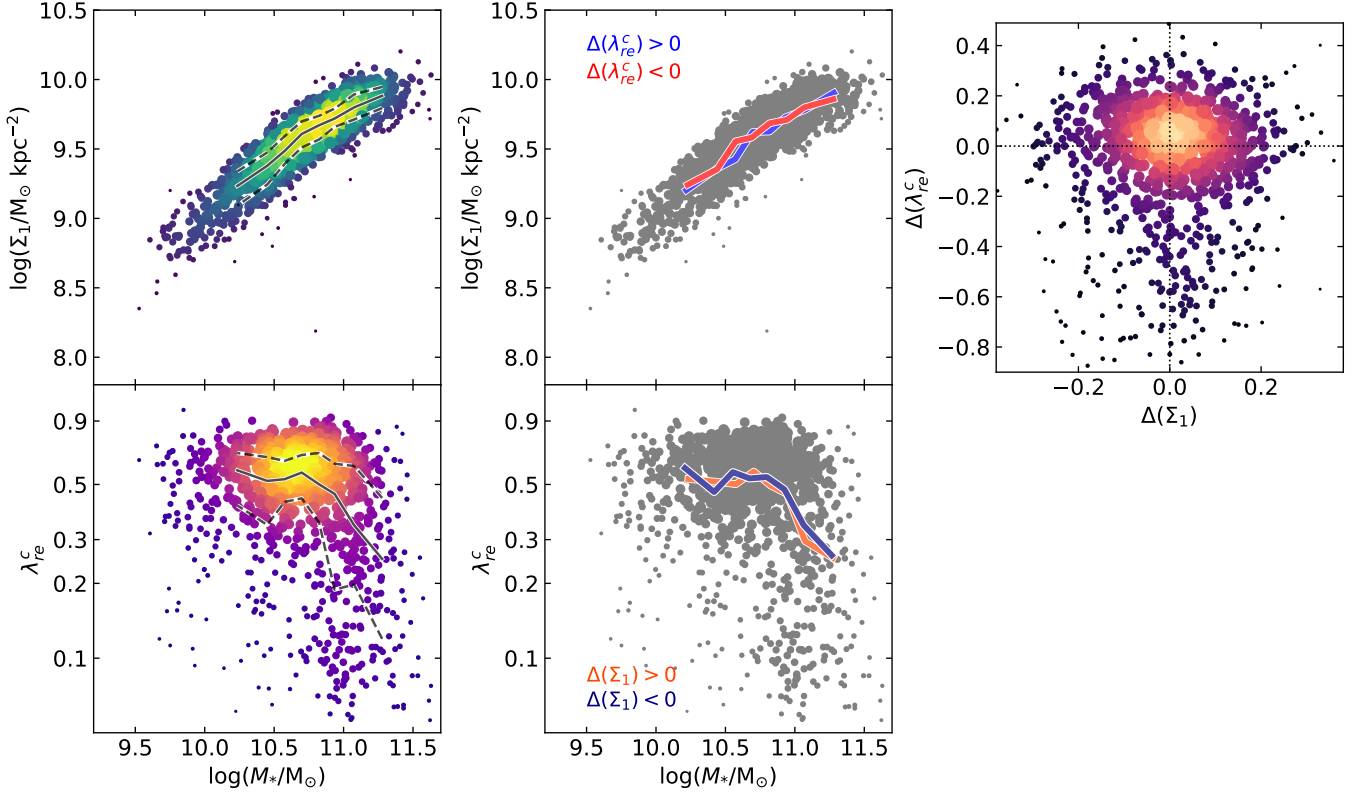


Figure 4. The correlation between Σ_1 and λ_{re}^c below the SFMS. Colors and symbols are as in Fig. 3. Contrary to what observed in star-forming galaxies, for passive systems we find no correlation between Σ_1 and λ_{re}^c at fixed stellar mass.

inter-quartile range IQR ~ 0.3 dex and 0.13 dex for the $\Sigma_1 - M_*$ and $\lambda_{re}^c - M_*$ relationships, respectively; see Table C1) and our goal is to establish whether higher central surface densities imply lower spins, and vice-versa. To do so, we start by quantifying the offset in Σ_1 and λ_{re}^c for every galaxy in our sample with respect to the median value observed for SFMS galaxies at fixed stellar mass. Specifically, for each galaxy, we define $\Delta(\Sigma_1)$ and $\Delta(\lambda_{re}^c)$ as the logarithmic difference between the observed value and the median value of Σ_1 or λ_{re}^c for all SFMS galaxies within 0.1 dex in stellar mass. In the top right panel of Fig. 3, we plot $\Delta(\lambda_{re}^c)$ vs. $\Delta(\Sigma_1)$ to show that the two quantities are clearly correlated (Spearman correlation coefficient $\rho \sim -0.30$, with a standard error from bootstrapping of 0.03). At fixed stellar mass, galaxies with higher Σ_1 show lower stellar spins, and vice-versa. This indicates that, once we control for stellar mass, an increase in central stellar surface density traces an increase in the importance of random motions in the gravitational support of galaxies, and thus most likely tracing the presence of small classical bulges (or potentially just the presence of a significantly thicker stellar disc). However, it is important to remind the reader that all these galaxies are rotationally-dominated, and that the decrease in spin is minimal, consistent with structural differences between those pure discs and galaxies with small bulge components (e.g., the equivalent of moving from Sd to Sb morphological types, e.g., Cortese et al. 2016; van de Sande et al. 2018; Falc3n-Barroso et al. 2019).

To show how the population of high/low Σ_1/λ_{re}^c populates the $\Sigma_1 - M_*$ and $\lambda_{re}^c - M_*$ scaling relations, respectively, in the middle column of Fig. 3 we show the running medians for galaxies with $\Delta(\lambda_{re}^c) > 0$ and $\Delta(\lambda_{re}^c) < 0$ on the $\Sigma_1 - M_*$ relation, and for galaxies with $\Delta(\Sigma_1) > 0$ and $\Delta(\Sigma_1) < 0$ on the $\Sigma_1 - M_*$ relation. In

both cases, galaxies with higher spin/ lower central surface densities (and vice-versa) map each other very well, and they follow parallel relations as a function of stellar mass. This confirms that the two observables are tracing the same structural changes *at fixed stellar mass*.

3.2 The passive population

The natural next step is to investigate whether or not the correlation between Σ_1 and stellar spin holds for galaxies that are no longer on the SFMS. A rapid glimpse at Fig. 4, which provides the same parametrisation presented in Fig. 3 but for passive galaxies, immediately shows that here the situation is dramatically different. The picture put forward in the subsection above may no longer be valid below the SFMS.

Starting from the $\Sigma_1 - M_*$ (top left) and $\lambda_{re}^c - M_*$ (bottom left) scaling relations, we see significant differences. First, as already known (e.g., Fang et al. 2013), at fixed stellar mass the range of Σ_1 observed in passive galaxies is significantly narrower (IQR ~ 0.19 dex) than that of star-forming systems. Second, and most importantly, the opposite happens for the stellar spin. The spread in λ_{re}^c at fixed mass increases by more than a factor of 2 (IQR increasing with mass from ~ 0.2 to 0.57 dex, see Table C1) and, if any trend is present, now spin clearly decreases with increasing stellar mass. However, this should not be interpreted as passive galaxies simultaneously growing their central surface density while losing their degree of rotational support. Indeed, as it is unlikely that passive galaxies grow significantly in mass via star formation, their mass increase must happen via mergers.

The chaotic nature of these processes, in particular in the case of major mergers, makes it unlikely that the scaling relations shown in the left column of Fig. 4 trace evolutionary tracks for passive galaxies.

The lack of a correlation between central surface density and spin becomes even more striking if we compare $\Delta(\Sigma_1)$ to $\Delta(\lambda_{re}^c)$. The only difference here is that the offsets are measured from the median values of the passive population at fixed mass. As shown in the right panel of Fig. 4, $\Delta(\Sigma_1)$ and $\Delta(\lambda_{re}^c)$ are no longer correlated ($\rho \sim -0.04 \pm 0.03$). Thus, there is no difference in average spin between galaxies with high and low stellar central surface density, and no difference in Σ_1 for galaxies with low and high spin at fixed mass. In other words, in the passive population, central surface density is not a good proxy for the kinematic state of the stellar population and, specifically, to gauge the balance between rotationally- and dispersion-supported structures within one effective radius. This result is not only driven by the presence of slow rotators, but it still holds if we focus on galaxies with $\lambda_{re}^c > 0.25$ ($\rho \sim -0.09 \pm 0.04$). Only once we focus our attention on galaxies with $\lambda_{re}^c > 0.4$, hints of a correlation between Σ_1 and λ_{re}^c start to re-emerge, but still with lower statistical significance than that observed for SFMS galaxies ($\rho \sim -0.22 \pm 0.03$).

In retrospect, and as already hinted in the introduction, this result should not come as a complete surprise. Already from a visual morphology point of view we know that, while star-forming galaxies are primarily disks, passive systems include pure discs, discs plus ‘bulges’ and pure ‘bulges’, with ‘bulges’ including both classical and pseudo-bulge structures. However, this morphological spread is not encapsulated by parameters that are sensitive to the 2D projected distribution of stars in galaxies, while they are clearly traced by stellar kinematic information such as the stellar spin parameter (e.g., Cappellari et al. 2011a; Krajnović et al. 2013; Cortese et al. 2016).

4 DISCUSSION

The main result of this work is the lack of a direct connection between central stellar surface density and stellar spin parameter across the entire SFR- M_* parameter space covered by nearby galaxies. For star-forming galaxies, differences in Σ_1 , at fixed mass trace changes in stellar kinematics. This correlation disappears below the SFMS. Here, Σ_1 cannot be used to infer the presence (and the importance) of classical bulges in passive galaxies. We can use these findings, combined with previous works, to improve our current understanding of how galaxies evolve from a structural point of view across the SFR- M_* plane.

Starting from Fig. 4, the striking difference in dynamic range between Σ_1 and λ_{re}^c at fixed stellar mass and the wide range (0.2–0.57 dex) in observed stellar spin imply that the passive population spans a variety of structural properties (and hence morphologies), significantly larger than what is observed in the star-forming galaxy population. Assuming that at higher redshift SFMS galaxies still show a small scatter in stellar spin at fixed stellar mass, our finding implies that during (or after) the quenching phase galaxies can experience a wide range of structural transformation, from remaining rotationally-dominated with relatively small classical bulges at their centre, up to becoming slow-rotators fully dominated by random motions, with this extreme case becoming relevant only at high stellar masses ($> 10^{10.5} M_\odot$, e.g., Guo et al. 2020; van de Sande et al. 2021).

It would be tempting to use our findings to question the notion of a single (or small number) of evolutionary paths towards quiescence for galaxies at $z \sim 0$ (e.g., Woo & Ellison 2019; Suess et al. 2021), and instead support a more complex picture with a diversity

of paths leading to quenching and structural transformation (Cortese & Hughes 2009; Fraser-McKelvie et al. 2018; Janowiecki et al. 2020; Cortese et al. 2021; Saintonge & Catinella 2022), which would also be in line with the diversity observed in stellar population properties of passive galaxies both in the local Universe and at higher redshift (e.g., Thomas et al. 2005; Graves et al. 2009; Tacchella et al. 2022). However, we cannot exclude that just mergers alone (i.e., minor and major mergers combined) may still explain the stellar kinematics properties of galaxies, with the wide range of spin simply due to the huge variety of, e.g., minor mergers that a galaxy can experience (see also Grand et al. 2017; Garrison-Kimmel et al. 2018), combined with the inevitable mass loss and associated adiabatic expansion (e.g., van Dokkum et al. 2014). Nevertheless, our results clearly demonstrate that the Σ_1 - M_* parameter space alone cannot be used to fully unveil the structural evolution of galaxies, and at least confirm that major/disruptive mergers become a significant pathway for galaxy transformation only in the very high stellar mass regime, where a statistically significant population of slow rotating galaxies starts to emerge.

Whether the structural transformation happens during or after quenching (Cortese et al. 2019), and if the same physical process is responsible for both, cannot be established from this analysis. However, a comparison between the range of Σ_1 and λ_{re}^c covered by the active and passive population, as shown in Figs. 3 and 4, suggests that the bulk of dispersion-supported cores in our sample do not form on the SFMS. In other words, we are not seeing major classical bulge growth on the SFMS, before quenching. Of course, there is a small fraction of star-forming galaxies that shows spin parameters consistent with a high degree of random motion (i.e., $\sim 10\%$ with $\lambda_{re}^c < 0.4$) but, as already shown by Fraser-McKelvie et al. (2021), these are primarily interacting systems and cannot, alone, explain the observed difference between the active and passive populations. Similarly, while the scatter in stellar spin observed in our SFMS sample indicates that galaxies may be growing dispersion-supported central structures in the SFMS, these remain a relatively small fraction of the total galaxy mass, and correspond to the typical population of early-type star-forming spirals observed in the local Universe (e.g., Cook et al. 2019; Falcón-Barroso et al. 2019). This is even more the case if we take into account the fact that small changes in λ_{re}^c in the SFMS may also trace the presence of a thick disc component, and not of a central dispersion-supported bulge, suggesting that our findings provide some conservative upper-limits on the importance of dispersion-supported bulges in the SFMS.

As discussed by Croom et al. (2021b) and Cortese et al. (2019), part of the differences in stellar spin between the active and passive populations could be due to a combination of size evolution and progenitor bias, as most of the quiescent systems in our sample left the SFMS a few billion years ago, at the very least. However, even ignoring this, we do not really see a large family of galaxies with kinematic properties consistent with the presence of prominent central massive classical bulges (e.g., $\lambda_{re}^c < 0.5$) on the SFMS (see also Morselli et al. 2017; Cook et al. 2020). Either most of classical bulges were formed at earlier epochs, via processes that have gradually become less efficient in recent times, or their mass growth takes place when (or after) galaxies have started leaving the SFMS. This is a key difference between using Σ_1 and λ_{re}^c as an indicator of structural transformation: i.e., while, when observed in two dimensions, all passive systems have similar central stellar surface densities consistent with that expected for classical bulge-dominated systems, from a stellar kinematic point of view they are far from being a homogeneous family, in particular for stellar masses greater than $\sim 10^{10.5} M_\odot$. An increase in central stellar surface density cannot be blindly

interpreted as evidence for an increase in the importance of random motions on the gravitational support of galaxies. Indeed, as shown in Fig. 3, on the SFMS, galaxies grow in both mass and central stellar surface density (Walters et al. 2021), but their stellar spin either remains constant or even slightly increases.

Excitingly, the potential disconnect between quenching and morphological transformation as well as the large variety of merger-driven kinematic changes in galaxies suggested here appear in line with predictions from large hydro-dynamical cosmological simulations such as EAGLE (e.g., Lagos et al. 2018, 2022) IllustrisTNG (e.g., Tacchella et al. 2019; Park et al. 2021). However, it is important to note that some of these findings may be affected by spurious collisional heating (Ludlow et al. 2021) and next generation/higher resolution runs are needed to fully confirm these scenarios and allow us to perform a quantitative comparison between observations and simulations (see also van de Sande et al. 2019).

The main limitation of our work is that we are not comparing stellar surface density and stellar spin for the same regions. While Σ_1 traces the inner 1 kpc, λ_{re}^c is measured within one effective radius, thus encapsulating a larger area (on average a factor of ~ 3 larger in radius for passive systems and ~ 4 for star-forming ones) and potentially more prone to trace changes in the outer parts of galaxies. Unfortunately, with current facilities, it is practically impossible to obtain higher spatial resolution IFS observations for ~ 1500 galaxies to quantify λ_{re}^c within 1 kpc. Thus, it is important to discuss if, and how, our conclusions may be affected by this issue.

On the SFMS, it is possible that the correlation between spin and central surface density becomes even stronger, but the main conclusion of star-forming galaxies remaining rotationally-dominated systems and having only small classical bulges would hold. Below the SFMS, it is difficult to think of a scenario in which the lack of correlation between Σ_1 and λ_{re}^c would only be due to the different apertures used to estimate the two quantities. This could only happen if the bulk of passive rotationally-dominated galaxies becomes consistent with being a slow rotator within 1 kpc. While a smaller aperture does imply a smaller rotational velocity and thus a narrower range of λ (assuming a flat velocity dispersion profile), it is unlikely that the scatter in spin at fixed mass decreases so much to become consistent, or even smaller, than that observed in the SFMS. Indeed, from previous studies of the radial cumulative distribution of spin parameter in early type galaxies, we know that the variety in spin parameter values is already present in the very inner parts of galaxies (e.g., Emsellem et al. 2011; Arnold et al. 2014; van de Sande et al. 2017).

What we have been able to test is whether our results hold if we use the stellar surface density within one effective radius (Σ_e instead of Σ_1 as a proxy for 2D structure). While, as already known, the scatter in the Σ_e - M_* relation is larger than what observed for the Σ_1 - M_* trend, we still find that Σ_e and λ_{re}^c trace each other on the SFMS while they are uncorrelated in the passive population.

Thus, despite the fact that the different apertures used in this work may affect the detailed quantification of the correlation between Σ_1 and λ_{re}^c , we expect that our main conclusion should qualitatively hold once measuring the spin parameter within 1 kpc for large statistical samples will become possible.

5 SUMMARY

In this paper, we have combined estimates of the 2D stellar surface density (Σ_1) of galaxies within their central 1 kpc, with measurements of their stellar spin parameter within one effective radius (λ_{re}^c), to

determine if changes in Σ_1 map variations in stellar kinematics. We showed that:

- On the SFMS, at fixed stellar mass, galaxies with higher Σ_1 have lower spin, and vice-versa, but the vast majority of star-forming galaxies are rotationally-dominated (i.e., discs) systems. While Σ_1 clearly grows with increasing stellar mass, the stellar spin either remains constant or increases by only $\lesssim 0.1$ dex over 1 dex in stellar mass.
- Below the SFMS, Σ_1 and λ_{re}^c are no longer correlated. Passive galaxies show a narrow range of Σ_1 but a wide range of λ_{re}^c values. Here, while Σ_1 still increases with increasing mass, λ_{re}^c decreases with mass, although with a large scatter.

Together, our findings imply that, in passive galaxies, the central stellar surface density cannot be used to disentangle rotationally- from dispersion-supported structures. In the context of galaxy evolution and structural transformation at $z \sim 0$, we interpret our results as follows:

- Only small classical bulges are able to grow while galaxies are on the SFMS. Major *compaction* episodes where dispersion-supported structures grow and create bulge-dominated star-forming systems are extremely rare at $z \sim 0$.
- If classical bulge formation is still efficient at $z \sim 0$, this takes place primarily during (or after) galaxies have started their quenching phase.
- Passive galaxies are, from a structural point of view, an heterogeneous population. While this may still be consistent with a two-way path towards quiescence, at this stage it cannot be excluded that a multitude of evolutionary paths (and potentially physical processes) are responsible for the transformation of active discs into quiescent systems.

ACKNOWLEDGEMENTS

We thank the anonymous referee for useful comments which improved the quality of this manuscript. This research was conducted by the Australian Research Council Centre of Excellence for All Sky Astrophysics in 3 Dimensions (ASTRO 3D), through project number CE170100013. LC acknowledges support from the Australian Research Council Discovery Project and Future Fellowship funding schemes (DP210100337, FT180100066). JvdS acknowledges support of an Australian Research Council Discovery Early Career Research Award (project number DE200100461) funded by the Australian Government. JBH is supported by an ARC Laureate Fellowship FL140100278. JJB acknowledges support of an Australian Research Council Future Fellowship (FT180100231). SMS acknowledges funding from the Australian Research Council (DE220100003). Parts of this work were performed on the OzSTAR national facility at Swinburne University of Technology. The OzSTAR program receives funding in part from the Astronomy National Collaborative Research Infrastructure Strategy (NCRIS) allocation provided by the Australian Government.

The SAMI Galaxy Survey is based on observations made at the Anglo-Australian Telescope. The Sydney-AAO Multi-object Integral field spectrograph (SAMI) was developed jointly by the University of Sydney and the Australian Astronomical Observatory. The SAMI input catalogue is based on data taken from the Sloan Digital Sky Survey, the GAMA Survey and the VST ATLAS Survey. The SAMI Galaxy Survey is supported by the Australian Research Council Centre of Excellence for All Sky Astrophysics in 3 Dimensions (ASTRO 3D), through project number CE170100013, the Australian Research

Council Centre of Excellence for All-sky Astrophysics (CAASTRO), through project number CE110001020, and other participating institutions. The SAMI Galaxy Survey website is <http://sami-survey.org/>

Funding for the Sloan Digital Sky Survey IV has been provided by the Alfred P. Sloan Foundation, the U.S. Department of Energy Office of Science, and the Participating Institutions.

SDSS-IV acknowledges support and resources from the Center for High Performance Computing at the University of Utah. The SDSS website is www.sdss.org.

SDSS-IV is managed by the Astrophysical Research Consortium for the Participating Institutions of the SDSS Collaboration including the Brazilian Participation Group, the Carnegie Institution for Science, Carnegie Mellon University, Center for Astrophysics | Harvard & Smithsonian, the Chilean Participation Group, the French Participation Group, Instituto de Astrofísica de Canarias, The Johns Hopkins University, Kavli Institute for the Physics and Mathematics of the Universe (IPMU) / University of Tokyo, the Korean Participation Group, Lawrence Berkeley National Laboratory, Leibniz Institut für Astrophysik Potsdam (AIP), Max-Planck-Institut für Astronomie (MPIA Heidelberg), Max-Planck-Institut für Astrophysik (MPA Garching), Max-Planck-Institut für Extraterrestrische Physik (MPE), National Astronomical Observatories of China, New Mexico State University, New York University, University of Notre Dame, Observatório Nacional / MCTI, The Ohio State University, Pennsylvania State University, Shanghai Astronomical Observatory, United Kingdom Participation Group, Universidad Nacional Autónoma de México, University of Arizona, University of Colorado Boulder, University of Oxford, University of Portsmouth, University of Utah, University of Virginia, University of Washington, University of Wisconsin, Vanderbilt University, and Yale University.

DATA AVAILABILITY

The data used for this work has been presented in [Fraser-McKelvie et al. \(2021\)](#) and [Woo & Ellison \(2019\)](#). The SAMI data cubes and value-added products used in this paper are available from Astronomical Optics' Data Central service at: <https://datacentral.org.au/>. The MaNGA data products are available at: <https://www.sdss.org/dr15/manga/manga-data/data-access/>.

AUTHOR CONTRIBUTION STATEMENT

LC devised the project and drafted the paper. AMF and JW performed the measurements of stellar kinematics and stellar surface density, respectively. LC, AMF, JW, BC and KH contributed to the initial data analysis and preliminary interpretation of the results. JvdS, JBH, JJB and SC provided key support to all the activities of the SAMI Galaxy Survey ('builder status'). All authors discussed the results and commented on the manuscript.

REFERENCES

- Arnold J. A., et al., 2014, *ApJ*, **791**, 80
 Barro G., et al., 2017, *ApJ*, **840**, 47
 Blanton M. R., Kazin E., Muna D., Weaver B. A., Price-Whelan A., 2011, *AJ*, **142**, 31
 Bryant J. J., et al., 2015, *MNRAS*, **447**, 2857
 Bullock J. S., Dekel A., Kolatt T. S., Kravtsov A. V., Klypin A. A., Porciani C., Primack J. R., 2001, *ApJ*, **555**, 240
 Bundy K., et al., 2015, *ApJ*, **798**, 7
 Cappellari M., Copin Y., 2003, *MNRAS*, **342**, 345
 Cappellari M., et al., 2011a, *MNRAS*, **413**, 813
 Cappellari M., et al., 2011b, *MNRAS*, **416**, 1680
 Chen Z., et al., 2020, *ApJ*, **897**, 102
 Cheung E., et al., 2012, *ApJ*, **760**, 131
 Cook R. H. W., Cortese L., Catinella B., Robotham A., 2019, *MNRAS*, **490**, 4060
 Cook R. H. W., Cortese L., Catinella B., Robotham A., 2020, *MNRAS*, **493**, 5596
 Cortese L., Hughes T. M., 2009, *MNRAS*, **400**, 1225
 Cortese L., et al., 2016, *MNRAS*, **463**, 170
 Cortese L., et al., 2019, *MNRAS*, **485**, 2656
 Cortese L., Catinella B., Smith R., 2021, *Publ. Astron. Soc. Australia*, **38**, e035
 Croom S. M., et al., 2021a, *MNRAS*, **505**, 991
 Croom S. M., et al., 2021b, *MNRAS*, **505**, 2247
 del Moral-Castro I., et al., 2020, *A&A*, **639**, L9
 de Vaucouleurs G., 1959, *Handbuch der Physik*, **53**, 275
 Emsellem E., et al., 2007, *MNRAS*, **379**, 401
 Emsellem E., et al., 2011, *MNRAS*, **414**, 888
 Erwin P., et al., 2015, *MNRAS*, **446**, 4039
 Falcón-Barroso J., et al., 2019, *A&A*, **632**, A59
 Fang J. J., Faber S. M., Koo D. C., Dekel A., 2013, *ApJ*, **776**, 63
 Fraser-McKelvie A., Aragón-Salamanca A., Merrifield M., Tabor M., Bernardi M., Drory N., Parikh T., Argudo-Fernández M., 2018, *MNRAS*, **481**, 5580
 Fraser-McKelvie A., et al., 2021, *MNRAS*, **503**, 4992
 Garrison-Kimmel S., et al., 2018, *MNRAS*, **481**, 4133
 Graham M. T., et al., 2018, *MNRAS*, **477**, 4711
 Grand R. J. J., et al., 2017, *MNRAS*, **467**, 179
 Graves G. J., Faber S. M., Schiavon R. P., 2009, *ApJ*, **693**, 486
 Guo K., et al., 2020, *MNRAS*, **491**, 773
 Harborne K. E., van de Sande J., Cortese L., Power C., Robotham A. S. G., Lagos C. D. P., Croom S., 2020, *MNRAS*, **497**, 2018
 Hardwick J. A., Cortese L., Obreschkow D., Catinella B., Cook R. H. W., 2022, *MNRAS*, **509**, 3751
 Hubble E. P., 1926, *ApJ*, **64**, 321
 Janowiecki S., Catinella B., Cortese L., Saintonge A., Wang J., 2020, *MNRAS*, **493**, 1982
 Kent S. M., 1985, *ApJS*, **59**, 115
 Kormendy J., Bender R., 2012, *ApJS*, **198**, 2
 Kormendy J., Kennicutt Jr. R. C., 2004, *ARA&A*, **42**, 603
 Krajnović D., et al., 2013, *MNRAS*, **432**, 1768
 Lagos C. d. P., et al., 2018, *MNRAS*, **473**, 4956
 Lagos C. d. P., Emsellem E., van de Sande J., Harborne K. E., Cortese L., Davison T., Foster C., Wright R. J., 2022, *MNRAS*, **509**, 4372
 Lange R., et al., 2016, *MNRAS*, **462**, 1470
 Ludlow A. D., Fall S. M., Schaye J., Obreschkow D., 2021, *MNRAS*, **508**, 5114
 Meert A., Vikram V., Bernardi M., 2015, *MNRAS*, **446**, 3943
 Mo H. J., Mao S., White S. D. M., 1998, *MNRAS*, **295**, 319
 Morselli L., Popesso P., Erfanianfar G., Concas A., 2017, *A&A*, **597**, A97
 Mosleh M., Tacchella S., Renzini A., Carollo C. M., Molaiezhad A., Onodera M., Khosroshahi H. G., Lilly S., 2017, *ApJ*, **837**, 2
 Noguchi M., 1999, *ApJ*, **514**, 77
 Oh S., et al., 2020, *MNRAS*, **495**, 4638
 Park M., et al., 2021, arXiv e-prints, p. [arXiv:2112.07679](https://arxiv.org/abs/2112.07679)
 Peng C. Y., Ho L. C., Impy C. D., Rix H.-W., 2002, *AJ*, **124**, 266
 Romanowsky A. J., Fall S. M., 2012, *ApJS*, **203**, 17
 Saintonge A., Catinella B., 2022, arXiv e-prints, p. [arXiv:2202.00690](https://arxiv.org/abs/2202.00690)
 Salim S., et al., 2016, *ApJS*, **227**, 2
 Simard L., Mendel J. T., Patton D. R., Ellison S. L., McConnachie A. W., 2011, *ApJS*, **196**, 11
 Suess K. A., Kriek M., Price S. H., Barro G., 2021, *ApJ*, **915**, 87
 Tabor M., Merrifield M., Aragón-Salamanca A., Fraser-McKelvie A., Penterken T., Smethurst R., Drory N., Lane R. R., 2019, *MNRAS*, **485**, 1546
 Tacchella S., et al., 2015, *Science*, **348**, 314

- Tacchella S., Dekel A., Carollo C. M., Ceverino D., DeGraf C., Lapiner S., Mandelker N., Primack Joel R., 2016, *MNRAS*, 457, 2790
- Tacchella S., et al., 2019, *MNRAS*, 487, 5416
- Tacchella S., et al., 2022, *ApJ*, 926, 134
- Thomas D., Maraston C., Bender R., Mendes de Oliveira C., 2005, *ApJ*, 621, 673
- van de Sande J., et al., 2017, *ApJ*, 835, 104
- van de Sande J., et al., 2018, *Nature Astronomy*, 2, 483
- van de Sande J., et al., 2019, *MNRAS*, 484, 869
- van de Sande J., et al., 2021, *MNRAS*, 508, 2307
- van Dokkum P. G., et al., 2014, *ApJ*, 791, 45
- Walters D., Woo J., Ellison S. L., Hani M. H., 2021, *MNRAS*, 504, 1677
- Wang E., Kong X., Pan Z., 2018, *ApJ*, 865, 49
- Wang B., Cappellari M., Peng Y., Graham M., 2020, *MNRAS*, 495, 1958
- Westfall K. B., et al., 2019, *AJ*, 158, 231
- Whitaker K. E., et al., 2017, *ApJ*, 838, 19
- Woo J., Ellison S. L., 2019, *MNRAS*, 487, 1927
- Woo J., Dekel A., Faber S. M., Koo D. C., 2015, *MNRAS*, 448, 237
- Woo J., Carollo C. M., Faber S. M., Dekel A., Tacchella S., 2017, *MNRAS*, 464, 1077
- York D. G., et al., 2000, *AJ*, 120, 1579
- Zhu L., et al., 2018, *MNRAS*, 473, 3000
- Zolotov A., et al., 2015, *MNRAS*, 450, 2327

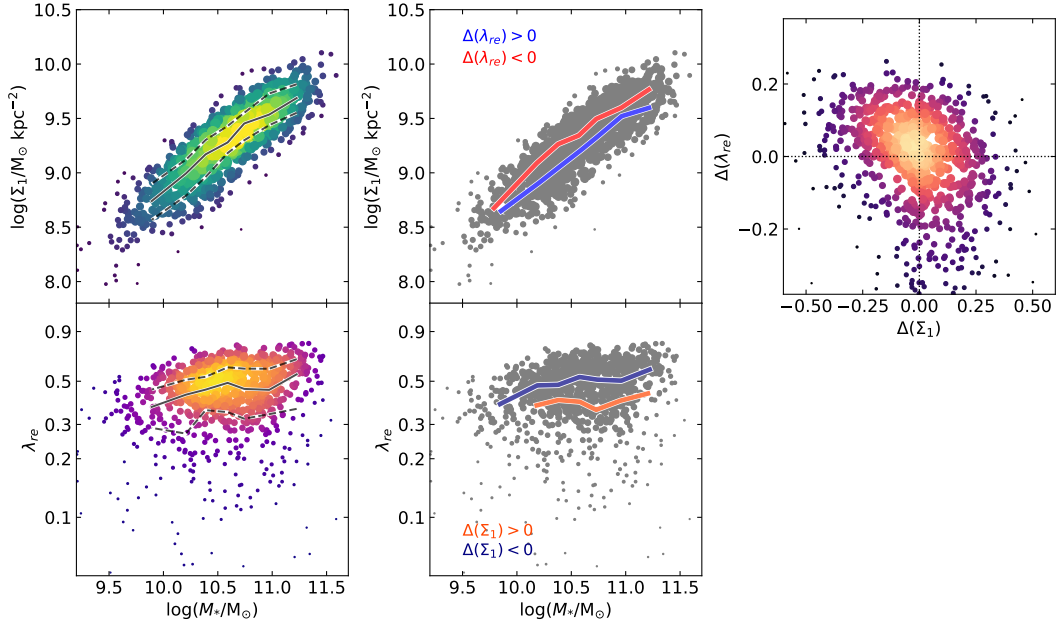


Figure A1. Same as Fig. 3, but with the observed λ_{re} plotted instead of the value corrected for both inclination and beam smearing.

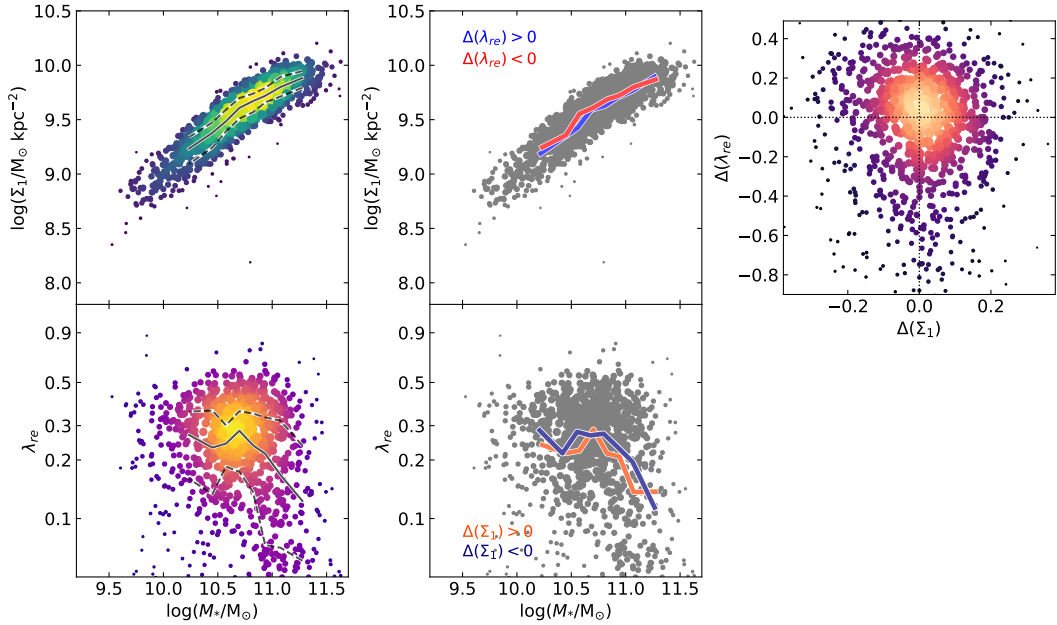


Figure A2. Same as Fig. 4, but with the observed λ_{re} plotted instead of the value corrected for both inclination and beam smearing.

APPENDIX A: EFFECT OF BEAM-SMEARING AND INCLINATION CORRECTIONS ON STELLAR SPIN

In the main body of this paper we have used λ_{re} values corrected for both inclination and beam smearing as a proxy for stellar spin parameter (λ_{re}^c). As extensively discussed in the literature (e.g., [Graham et al. 2018](#); [Harborne et al. 2020](#); [Fraser-McKelvie et al. 2021](#); [van de Sande et al. 2021](#)), for IFS surveys such as SAMI and MaNGA these corrections combined can easily change the value of λ_{re} by $\sim 50\%$ or more. Thus, it is important to make sure that the main conclusions of this paper are not driven by potential systematic effects in the correction themselves, but are still visible in the original measurements. With this aim, in Fig. A1 and A2 we reproduce Fig. 3 and 4 by using the observed value of λ_{re} instead of λ_{re}^c . As expected, values of spin parameter are lower and the scatter in the λ_{re} - M_* relations for both active and passive galaxies increase (average IQR ~ 0.23 and ~ 0.45 dex, respectively). This is due to the large variety of inclinations and observing conditions for the two samples. However, the lack of correlation between λ_{re} and Σ_1 ($\rho \sim -0.09 \pm 0.04$) and larger scatter in the λ_{re} - M_* relation for passive galaxies with respect to galaxies on the SFMS still remains. As such, we can conclude that our results are not qualitatively affected by the beam smearing and inclination corrections applied in this work.

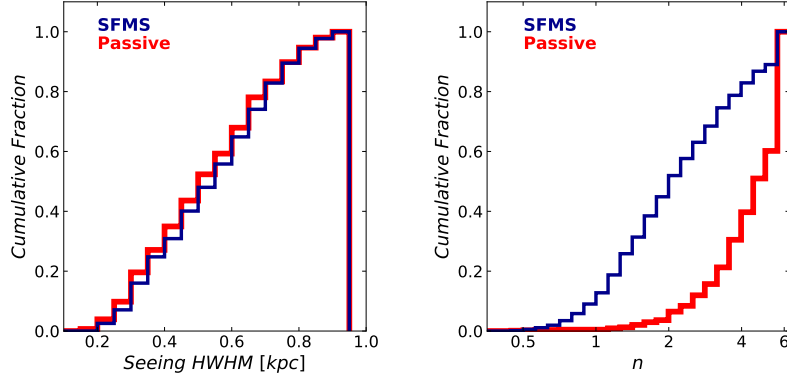


Figure B1. Cumulative distributions of seeing half-width-at-half-maximum (HWHM) in physical units (left) and Sersic indices (right) for SFMS (blue) and passive galaxies (red).

APPENDIX B: EFFECT OF SEEING ON THE ESTIMATE OF Σ_1

Σ_1 can be affected by seeing and, while our sample selection ensures that the half-width-at-half-maximum (HWHM) of the SDSS observations is always smaller than 1 kpc, it is important to briefly discuss if this might affect our main conclusions. Indeed, Barro et al. (2017) have shown that, even when the nominal resolution of the data is 0.6-0.7 kpc, Σ_1 could be systematically underestimated and that this effect is stronger for galaxies with higher Sersic index. Thus, the lack of correlation between $\lambda_{r_e}^c$ and Σ_1 in passive galaxies could just be the by-product of a larger effect of the atmospheric smearing in these galaxies. Unfortunately, empirical corrections for the effect of seeing applicable to our sample are not available. So, we cannot perform the same test presented in Appendix A. Nevertheless, we can use the work of Barro et al. (2017), combined with the properties of our sample, to discuss the potential role of seeing in our findings. In Fig. B1 we show the cumulative distributions of HWHM for the SDSS data used to estimate Σ_1 in physical scales (left) and of Sersic index (right) for our SFMS (blue) and passive population (red). Passive galaxies have the same HWHM distribution as SFMS objects and, if anything, they are marginally better resolved. In addition, as expected, passive systems cover a significantly narrower range of Sersic indices than active galaxies.

According to Barro et al. (2017, see their Fig. 14), at fixed HWHM, the effects of seeing on Σ_1 correlate strongly with Sersic index, so that a population covering a narrow range of Sersic indices will be all affected in a similar way, whereas for a sample spanning a wide range of Sersic indices the changes in Σ_1 may vary significantly (up to ~ 0.3 dex in the most extreme cases) from galaxy to galaxy. As such, given that our SFMS spans a significantly larger range of Sersic indices than the passive population, we should expect this family to be potentially more affected by atmospheric blurring and any secondary trends to be washed away. Conversely, we still find secondary trends for the SFMS population, making it unlikely that the lack of correlation between Σ_1 and $\lambda_{r_e}^c$ for passive galaxies is just an artefact of the limited spatial resolution of our data (see also the discussion of seeing effects in Woo et al. 2015). Lastly, we note that we have also tested our results by focusing on a sub-sample with $\text{HWHM} < 0.5$ kpc and our results are unaffected but, due to the significantly smaller number statistics, the quantification of trends as a function of mass and $\Delta(\Sigma_1)$ or $\Delta(\lambda_{r_e}^c)$ becomes highly uncertain, with only two bins of stellar mass having enough galaxies. This is why, contrary to what done in Appendix A, we do not show the equivalent of Fig. 3 and 4 for this subsample.

Table C1. The median Σ_1 and $\lambda_{r_e}^C$ per bin of stellar mass for SFMS and passive galaxies. Uncertainties indicate the 75% and 25% percentiles.

$\log(M_*/M_\odot)$	$\log(\Sigma_1/M_\odot \text{ kpc}^{-2})$	$\log(\lambda_{r_e}^C)$
Star – forming main sequence galaxies		
9.89	$8.74^{+0.16}_{-0.17}$	$-0.20^{+0.05}_{-0.09}$
10.21	$8.99^{+0.13}_{-0.20}$	$-0.17^{+0.06}_{-0.09}$
10.39	$9.17^{+0.13}_{-0.21}$	$-0.15^{+0.04}_{-0.08}$
10.59	$9.28^{+0.15}_{-0.10}$	$-0.14^{+0.05}_{-0.05}$
10.74	$9.45^{+0.10}_{-0.15}$	$-0.14^{+0.05}_{-0.09}$
10.97	$9.54^{+0.19}_{-0.10}$	$-0.15^{+0.05}_{-0.06}$
11.22	$9.69^{+0.13}_{-0.14}$	$-0.10^{+0.03}_{-0.08}$
Passive galaxies		
10.23	$9.23^{+0.11}_{-0.14}$	$-0.24^{+0.07}_{-0.14}$
10.45	$9.38^{+0.10}_{-0.13}$	$-0.29^{+0.10}_{-0.18}$
10.58	$9.49^{+0.11}_{-0.09}$	$-0.28^{+0.07}_{-0.09}$
10.70	$9.61^{+0.09}_{-0.10}$	$-0.25^{+0.07}_{-0.10}$
10.82	$9.67^{+0.07}_{-0.10}$	$-0.30^{+0.13}_{-0.15}$
10.94	$9.72^{+0.07}_{-0.06}$	$-0.34^{+0.12}_{-0.39}$
11.08	$9.80^{+0.09}_{-0.09}$	$-0.47^{+0.24}_{-0.24}$
11.28	$9.88^{+0.06}_{-0.09}$	$-0.60^{+0.25}_{-0.32}$

APPENDIX C: THE Σ_1 - M_* AND λ_{RE}^C - M_* RELATIONS FOR STAR-FORMING MAIN SEQUENCE AND PASSIVE GALAXIES

In Table C1 we present the median values (as well as 25% and 75% percentiles) for Σ_1 and $\lambda_{r_e}^C$ per bin of stellar mass. Each bin contains 100 galaxies. As discussed in § 2, we use Eq. 1 to separate star-forming from passive galaxies, labelling as passive all systems below -0.5 dex from the locus of the SFMS.

This paper has been typeset from a $\text{\TeX}/\text{\LaTeX}$ file prepared by the author.